Title

Enhanced Charge Carrier Transport in 2D Perovskites by Incorporating Single-Walled Carbon Nanotubes or Graphene

Journal

ACS Energy Letters, 5(1)

ISSN

2380-8195

Authors

de la Fuente, Mauricio Solis
Kaur, Sumanjeet
Hu, Qin
et al.

Publication Date

2020-01-10

DOI

10.1021/acsenergylett.9b01821

Peer reviewed

Enhanced charge-carrier transport in 2D perovskites by incorporating single-walled carbon nanotubes or graphene

Mauricio Solis de la Fuente[1], Sumanjeet Kaur[1*], Qin Hu[2,3], Edward Barnard[4], Peter Dudenas[1,5]*

Ahmet Kusoglu[1], Thomas P. Russell[2,3], Jeffrey J. Urban[4], Ravi Prasher[1]

[1]Energy Technology Division, Lawrence Berkeley National Laboratory, Berkeley, California 94720, USA.

[2]Materials Sciences Division, Lawrence Berkeley National Laboratory, Berkeley, California 94720, USA

[3]Department of Polymer Science and Engineering, University of Massachusetts, Amherst, Massachusetts 01003, USA

[4]The Molecular Foundry, Lawrence Berkeley National Laboratory, Berkeley, California 94720, USA.

[5]Department of Chemical and Biomolecular Engineering, University of California, Berkeley, California 94720, USA

AUTHOR INFORMATION

Corresponding Author

Mauricio Solis de la Fuente (msf@ier.unam.mx), Sumanjeet Kaur (skaur1@lbl.gov)

ABSTRACT. Two-dimensional (2D) organic-inorganic (hybrid) perovskites are considered promising candidates to replace conventional three-dimensional (3D) perovskites for solar cell applications as they have good resistance against moisture and UV light. However, the use of 2D perovskite is associated with a significant decrease in power efficiency resulting from their low photogenerated charge carrier density and poor charge transport. To improve power efficiency in 2D perovskites, highly crystalline films (near-single-crystal quality) of 2D perovskite needs to be synthesized where the alignment of the inorganic perovskite components is controlled to have vertical alignment with respect to the contacts to improve charge transport. In this work, we explored strategies to overcome this limitation, by integrating 2D perovskite with single-walled carbon nanotubes or graphene to enable more efficient extraction of charge carriers toward electric contacts. Longer carrier lifetimes were achieved after the incorporation of the carbon nanostructures in the films and at cell level, power efficiency increased by two-fold.

TOP-GRAPHIC

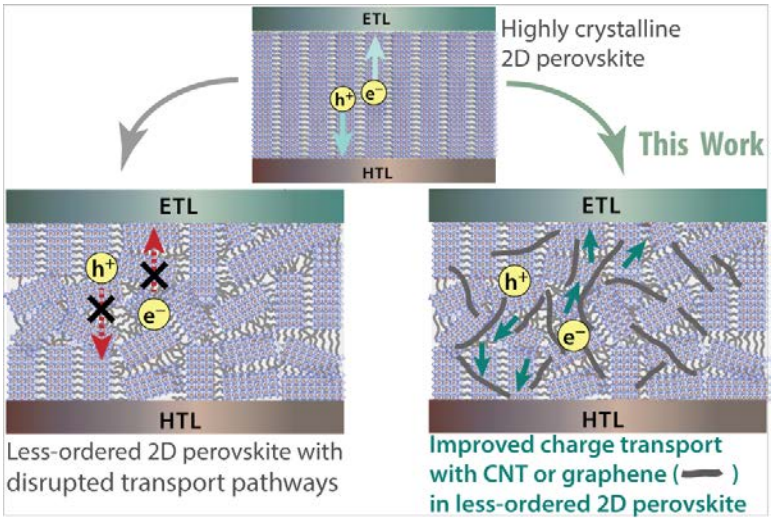

Three-dimensional (3D) organic-inorganic (hybrid) perovskites have been intensively investigated as photovoltaics owing to their excellent optoelectronic properties (strong absorbance, long diffusion length, fast carrier mobility). Significant progress has been made in their solar to electrical power conversion efficiencies, which increased from ~3.8% in 2009 to 23.7% by 2018[1]. However, their long-term stability under external agents, such as ultraviolet (UV) light, oxygen, humidity, and heat[2-4] is still an issue. In contrast to 3D perovskites, two-dimensional (2D) hybrid perovskites $A'_2A_{n-1}M_nX_{3n+1}$ have shown to exhibit more operational stability under environmental conditions than 3D perovskites (AMX_3), where A' is a long organic cation (spacer), A is a short organic cation, M is a divalent metal, and X is a halide. The long organic cations A' in 2D perovskites act as barriers to moisture because of their intrinsic hydrophobicity, reducing the vulnerability of the perovskite to humidity[5]. In addition, ion migration is also reduced, especially in low-dimensional systems where $n \rightarrow 1$, overcoming the illumination instability.[6] Although these advantages of 2D perovskites are promising for solar cell applications, they come at the expense of a significant decrease in power efficiency.[7] Certain limitations of 2D perovskites have been identified, including less efficient electronic transport through the structure due to the long organic chains, which present resistance to the motion of charge carriers and can be visualized as transport across potential barriers.[8] Thus the orientation of organic and inorganic components with respect to the current collectors becomes very crucial; with the vertical orientation being more efficient as it provides direct pathways for free carrier transport as shown in Figure 1A. Therefore, significant research has thus been focused on the synthesis of highly ordered 2D perovskite where the alignment of the inorganic perovskite components during synthesis process is controlled to have a preferential out-of-plane alignment (vertical alignment) with respect to the contacts in the solar cells.[9] Typical synthesis methods to

obtain preferential orientation include hot casting technique[9,10], the use of additives such as ammonium thiocyanate during spin coating[11], or the use of second spacer in the precursor solution.[12] While this has resulted in an increase in the power efficiency in small samples, scaling it up requires producing highly crystalline (near-single-crystal quality) 2D perovskite films by controlling process parameters during the synthesis process. Surprisingly, limited research has focused on improving carrier transport in less ordered 2D perovskite (Figure 1B) by incorporating other media such as, nanotubes or graphene, for hole and electron transport (Figure 1C). For 2D perovskites, it has been reported that they have higher exciton binding energy (E_B) than for their 3D counterparts owing to the quantum and dielectric confinements and hence require more energy to produce free carriers.[13] These confinements become stronger in low-dimensional systems and have a significant effect on the recombination processes.[14] However efficient internal exciton dissociation has been observed in 2D perovskites for $n > 2$, indicating that the presence of larger edge states can contribute to the generation of free carriers with longer lifetime.[15] Consequently the creation of paths by using carbon nanotubes or graphene (for example) that allows charge carriers to reach the electric contacts before recombining is essential to obtain efficient 2D perovskite solar cells.

Allotropes of carbon such as nanotubes or graphene have been used as hole and electron transport media in 3D halide perovskite because of their excellent transport properties, hydrophobicity, large surface area, and optical transparency.[16,17] The charge-transfer dynamics at the interface of hybrid perovskite/single-walled carbon nanotubes (SWCNTs) were studied, demonstrating that the energy level alignment for a type-II heterojunction and the band bending induced in the SWCNT layer promoted efficient hole extraction.[18] In addition, an increase in the carrier mobility (for both electrons and holes) of up to two orders of magnitude was reported in a

3D halide perovskite under illumination after SWCNTs were embedded in the perovskite structure.[19] Graphene (G) is also often used as a transparent electric contact because of its high electronic carrier mobility with light transmittance.[20] Recently, graphene nanofibers were added to hybrid perovskite solutions, with improvements in the carrier transport times associated with the effective electron transport.[21] Here, we explore modes to improve charge-carrier transport in less-ordered 2D perovskite $BA_2MA_3PbI_4I_{13}$ using nano materials (SWCNTs and graphene) which could provide connectivity between different inorganic domains and/or between inorganic domains and current collector (Figure 1C). We investigated the effect of nano material integration on morphology and structure of 2D perovskite films and correlated these findings with the optoelectronic changes, which are validated by monitoring the performance of solar cell devices.

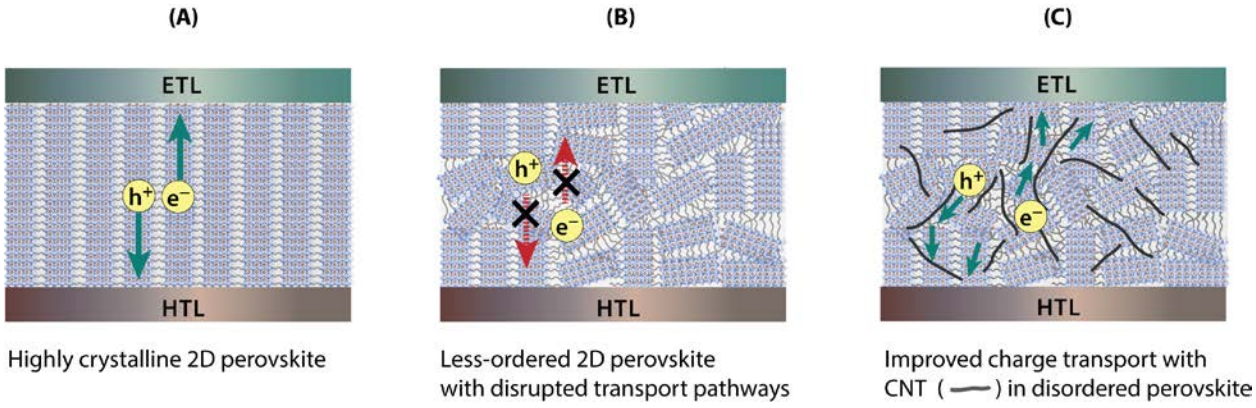

Figure 1: Charge transport dependence on orientation. A) Strong vertical alignment in 2D perovskite provides direct pathways for electron and hole extraction whereas with random orientation (B) Extraction of hole and electrons get hindered with presence of long organic insulating cations. C) Improving charge transport in less ordered 2D perovskite by incorporating CNT (or graphene), which allows for pathways for electron and hole transport between inorganic domains.

We prepared SWCNT–$BA_2MA_3PbI_4I_{13}$ and graphene–$BA_2MA_3PbI_4I_{13}$ composites using commercial semiconductor SWCNTs (0.78-nm diameter, 1-μm length) and graphene (thickness of 0.6–1.2 nm, flake diameter of 0.4–5 μm) respectively, which were previously dispersed in dimethylacetamide by sonication (30 min). The same molar concentration was used (10 mM) for both solutions, which were stable for several days. The films were fabricated following Chen's method to obtain the $BA_2MA_3PbI_4I_{13}$ perovskite (2D) with post-crystallization annealing.[9] We also deposited a 3D hybrid perovskite $CH_3NH_3PbI_3$ (3D) using a previously described procedure.[22] Inverted planar solar cell devices with the structure ITO/PEDOT:PSS/perovskite/PCBM/C_{60}/Al were fabricated; more details are provided in the experimental section.

Optical measurements of the 3D perovskite (PS 3D), 2D perovskite (PS 2D), 2D perovskite with SWCNTs (PS 2D-NT) and 2D perovskite with graphene (PS 2D-G) are shown in Figure 2. No significant differences were observed in the absorbance spectra of PS 2D-NT, PS 2D-G, and PS 2D (Figure 2A), with similar excitonic peak positions at 1.93, 2.04, and 2.16 eV, consistent with previously reported works.[13,23] A strong effect of the structure, including the organic cation length[24] and the number of inorganic slabs (n),[25,26] on the peaks was observed, with smoother (smaller) peaks observed with increasing n; this result is consistent with the absence of peaks in the PS 3D spectra. Absorption steady-state photoluminescence (PL) measurements were performed and a small shift was observed in the principal excitonic peak of PS 2D-NT (1.62 eV) and PS 2D-G (1.63 eV) when compared to PS 2D (1.65 eV) in the spectra. It is possible that the presence of the nanotubes and graphene (Figure 2B), which can induce lattice deformations, resulted in shifts in the radiative energy light emission peak; however, a more in-depth study is required. Further, time resolved photo luminesce decay measurements

were carried out on these samples to understand effect of these additions on the carrier lifetimes. The data is shown in Figure 2C where the charge-carrier lifetime τ was determined by fitting a bi-exponential function. A substantial difference in the kinetics of recombination was observed for the samples in the transient PL decay (Figure 2C) at the laser excitation of 500 nm. The thickness of film for all samples was ~200 nm. This could be due to PS 2D and PS 2D-G decay occurred via bimolecular recombination (fast recombination events), whereas the decay for PS 3D appeared to be monomolecular. PS 2D-NT showed contributions from both monomolecular and bimolecular recombination, where the electronic trap density and nature govern the recombination process of excited carriers.[27,28]

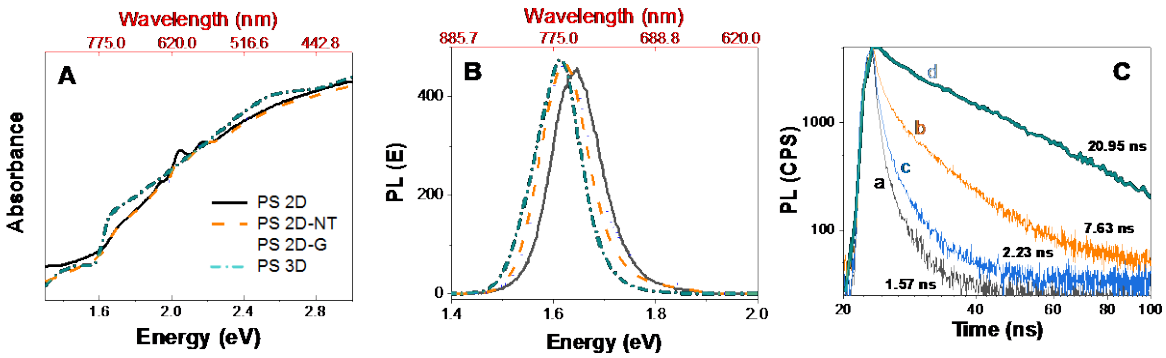

Figure 2. Optical measurements in hybrid perovskites: (A) Absorbance spectra, (B) normalized external photoluminescence, and (C) time-resolved photoluminescence decay of (a) PS 2D, (b) PS 2D-NT, (c) PS 2D-G, and (d) PS 3D.

Since it is possible that the addition of nanostructures could have changed the layer arrangements resulting in increased carrier lifetime, we prepared control samples using inert material (alumina nanoparticles (<50 nm)) that could not participate in charge transport but could still affect the layer arrangements. We used similar mole fraction as used for SWCNTs or graphene. The photo luminesce decay from these control samples (Figure S1) showed no change in carrier lifetime

emphasizes that the longer carrier lifetime in case of PS 2D-NT or PS 2D-G is mostly due to better charge transport. It should be noted that similar effects from some carbon nanostructures, such as fullerenes (PCBM), have been shown to be effective traps and grain-boundary passivators when embedded in 3D perovskites, permitting the achievement of longer carrier lifetimes.[27]

Inclusion of carbon nanotubes and graphene changed the film's overall opto-electronic properties, however the large area "bulk" measurements presented in Figure 2 do not reveal whether this effect was homogeneous or not. Scanning electron micrographs shown in Figure 3A (top row) indicate morphological variations on the micrometer length-scales for PS 2D-G and PS 2D-NT samples when compared to PS 2D. This could be either due to film thickness variations or phase separation due to the addition of CNT or graphene. We hypothesized that the film may have phase separated into 2D regions with no added carbon, and 3D-like regions with the graphene or SWCNTs. This separation could cause spatial variations in optical properties, i.e. areas of longer lifetime and blue-shifted emission. Thus, it is essential to carry out two-dimensional mapping of the opto-electronic properties of the film. We performed fluorescence spectrum and lifetime mapping with a custom optical microscope.[29] From these maps, shown in Figure 3A, there is only subtle or no spatial variation at the diffraction-limited resolution (~500 nm) of this microscope. In other words, we do not see micrometer-scale heterogeneous clustering of optical properties that would indicate phase separation. Note that heterogeneity at size-scales smaller than this optical diffraction limit cannot be ruled out from this measurement. From these maps we observe a distribution (Figure 3B) of PL peak energies that are relatively narrow and follow the trends seen in the bulk measurements (compare to Figure 2B). The lifetime distributions (Figure 3C) also follow the same trends as see in the bulk measurements in

Figure 2C. While their trends match, PL energies and lifetimes both are numerically different in these maps compared to bulk measurements likely due to the differences in carrier injection regime and laser repetition rate differences between experiments. The numerical trends for bulk and mapping measurements are summarized in Table S1.

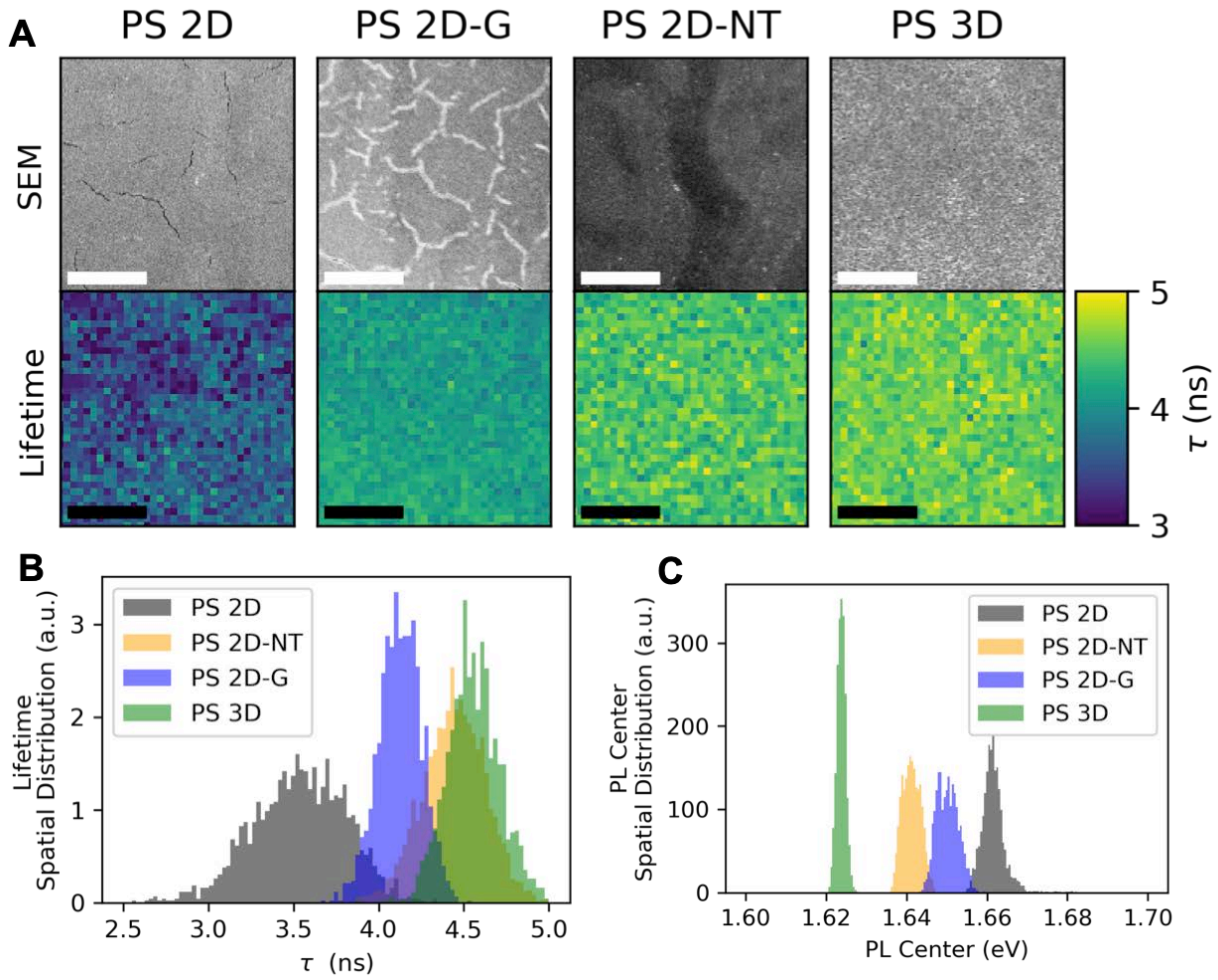

Figure 3. (A) SEM micrographs, and lifetime maps from the four types of samples. Spatial distributions of lifetime (B) and PL emission center energy (C) as measured by optical spectroscopy maps in (A). Scale bar is 5 µm.

To investigate the structural changes after incorporation of the SWCNTs or graphene in the 2D perovskite matrix, both grazing-incidence small angle X-ray scattering (GISAXS) and grazing-incidence wide-angle X-ray diffraction (GIWAXS) analysis were performed. Results from GISAXS are included in the supplementary information (Figure S2), where similar broad peaks with a spacing of 7–8 nm were observed for all of the materials and therefore we focus on crystallite structure obtained using GIWAXS to elucidate the structural origins of the observed material behavior. Figure 4 shows GIWAXS results of the perovskite samples. The diffraction rings of the 3D perovskite sample in Figure 4A indicate an isotropic distribution of crystallites. In contrast, all the 2D perovskite samples exhibited discrete Bragg spots, whose positions match literature values for these materials.[9,30] The incorporation of SWCNTs or graphene does not appear to change the crystal structure of these 2D perovskites, but does have an slight effect on grain size and orientation of the crystallites. To characterize the change in grain size, linecuts of the <111> peak were taken as a function of *q* and fit to extract FWHM. The <111> peak occurs through plane, and the FWHM in q_{FWHM} is inversely proportional to the through-plane crystallite grain size, important for vertical charge transport. The addition of SWCNTs causes an increase in vertical grain size relative to the neat 2D perovskite (Fig 4B). Furthermore, to characterize the orientational distribution of crystallites, azimuthal cuts of the <002>/<200> peak were taken versus χ (SXX) and fit to extract an angular FWHM, χ_{FWHM}. Contrary to the vertical grain size, SWCNTs slightly disrupts orientational order, showing a slightly larger FWHM in χ. On the other hand, graphene exhibits lower FWHM in χ relative to the neat sample suggesting more oriented structure and relatively less effect on the grain size. We compared grain size and crystallite orientation order of our samples with that of highly oriented 2D perovskite (PS 2D-HO) in Figure 4B and 4C, the data for which was obtained from Chen et al work.[9]When

compared with PS 2D-HO, all our samples have smaller grain sizes and less orientation order. However, some changes in the grain size or orientation order were observed after SWCNTs or graphene addition that could impact charge transport favorably, a more systematic study is required to isolate impact of each of this parameter on charge transport.

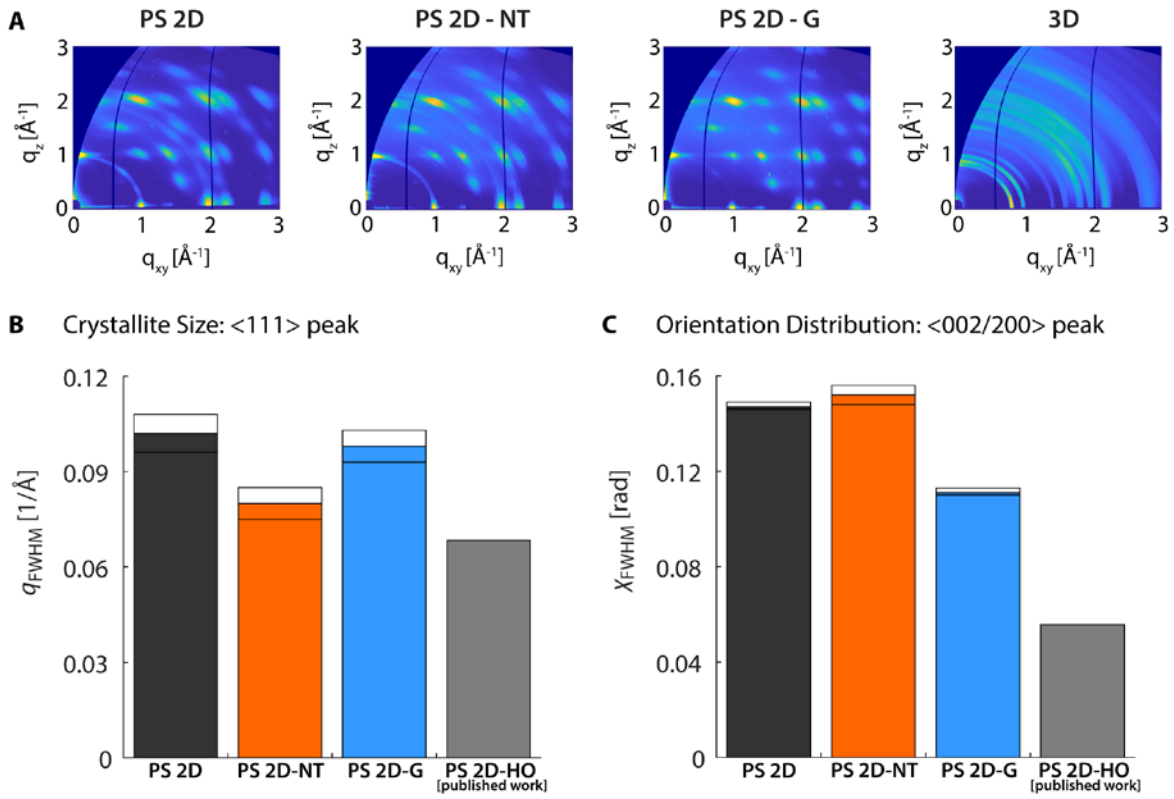

Figure 4. GIWAXS results for perovskite samples. (A) 2D scattering images of PS 2D, PS 2D-NT, PS 2D G, and PS 3D. (B) FWHM of the <111> peak in q. FWHM is inversely proportional to crystallite grain size; a lower FWHM indicates a larger crystallite size (C) FWHM of the <002>/<200> peak in χ. A smaller FWHM in χ indicates the material has higher orientational order. The data for highly oriented 2D perovskite (PS 2D-HO) obtained from Chen et al.[9] is also included in B and C for comparison.

After characterizing PS 2D, PS 2D-NT and PS 2D-G films, 40 solar cells of each type were prepared following the procedure reported by Chen et al.[7] (see experimental extended methods). Various device level characterizations were carried out to understand the effect of SWCNTs/graphene on 2D perovskite. Figure 5 summarizes the performance of PV devices. JV curves in Figure 5A showed increased current density for the PS 2D-NT and PS 2D-G when compared with that of PS 2D. Scan-dependent bias is presented in Figure S3 to discard improvements due to hysteresis behavior. For all devices JV curves were obtained at slow scan rate of 10mV/s. This has been reported to exhibit similar values as obtained at steady state measurements[31]. Increased current density with additives is consistent with the longer lifetimes and large grain sizes observed esp. for PS 2D-NT. Various concentrations of SWCNT solutions were explored to reach the optimal solar cell performance, the data for which is summarized in Figure S4. The photocurrent improvements can be attributed to one or combination of these factors: a) higher charge generation or b) faster transport or extraction of the carriers. To observe the effect of SWCNTs or graphene addition on charge generation, Ultraviolet Photon Spectroscopy (UPS) was carried out (Figure S5). No significant differences were observed in the valence band energy position for these samples. Similarly, the absorption spectra (Figure 2A) from all the samples showed no significant differences. Based on these measurements we believe that the charge generation is same across all the samples and the increase in photocurrent is due to improved charge transport. This is in agreement with the longer lifetimes observed in PS 2D-NT or PS 2D-G as shown in Figure 2C. We think that incorporating the nanotubes or graphene helped the charged carriers to overcome a barrier induced by organic spacers. It is plausible that the charge carriers might have been trapped in various domains (due to organic spacers) and incorporating SWCNTs or graphene opened pathways for charge carrier to reach hole or electron

transport layers as they provided bridges between various domain as illustrated in Figure 1C. Furthermore, the lower series resistance (slope dV/dJ) near open-circuit voltage in the case PS 2D-NT and PS 2D-G indicates that the carriers are now able to go through a less resistive path enabled by incorporation of these additives compared to the 2D perovskite. Since the Voc for all the samples remained the same, we believe that the SWNT/graphene addition did not result in a short circuit between HTL and ETL layers as it has been shown that short circuit would significantly reduce Voc.[32]

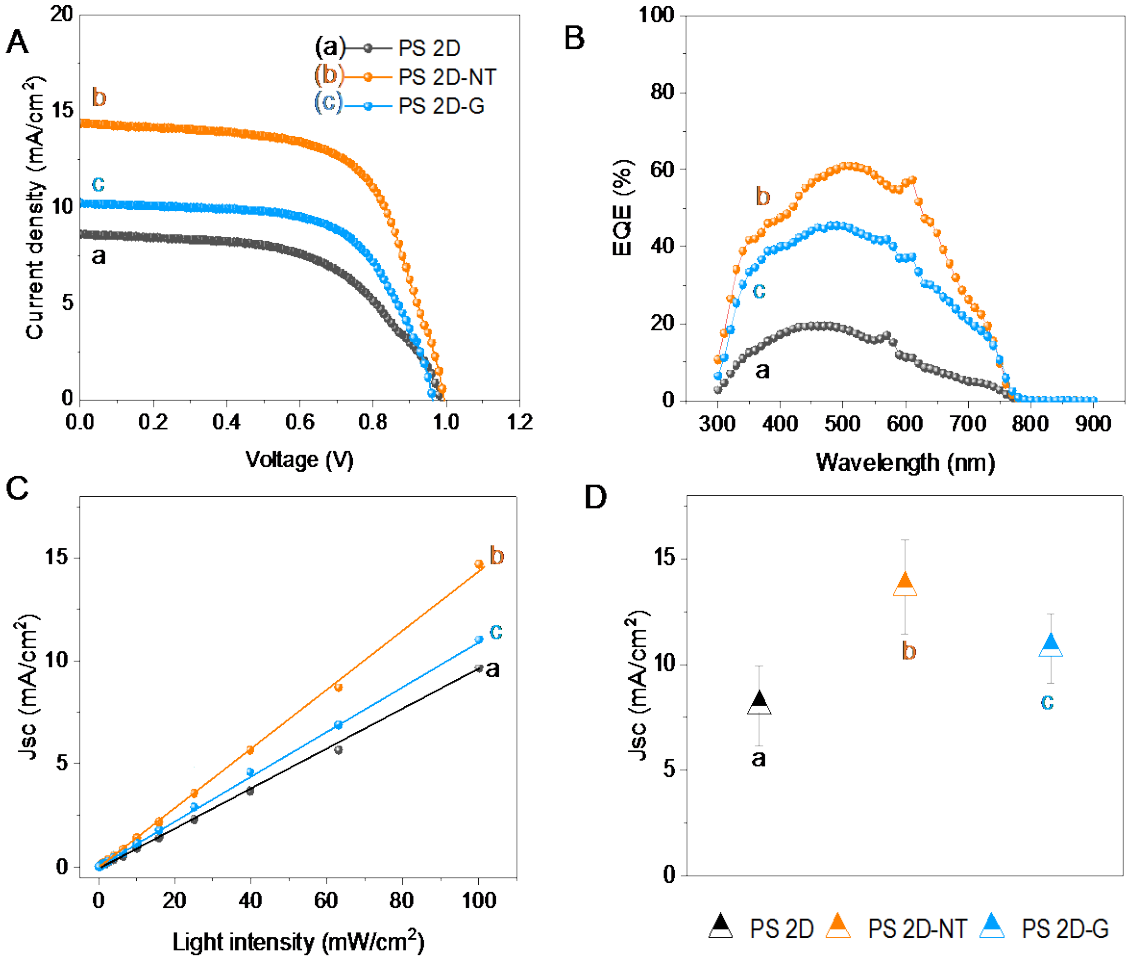

Figure 5. Performance of PV devices: A) Current density- voltage curves, B) External quantum efficiency EQE measurements, C) Variation of short-circuit current density (Jsc) with light intensity and D) Statistical data on short circuit current density (Jsc) from 40 solar cells of each type.

External Quantum Efficiency (EQE) measurements corroborates the increments in photocurrent in PS 2D-NT and PS 2D -G with respect to the pristine perovskite PS 2D, the data is shown in Figure 5B. To obtain information about the recombination process in the PV devices, measurements were performed at various light intensities in our devices. All the samples showed a linear dependence of $J_{sc} \propto I$ (light intensity), as observed in Figure 5C. As a direct relation of carrier generation, improved extraction of charge carriers toward electric contacts was observed in PS 2D-NT relative to that in PS 2D-G and PS 2D. However, no significant differences between samples were observed in open-circuit voltage (Voc) and shunt resistance (R_{sh}) under various light intensities (Figure S6) suggesting that the recombination processes are mostly similar for all the samples. The current densities from 40 solar cells (of each type) is shown in Figure 5D that highlights the similar trend as shown in Figure 5A. Table 1 represents the PV parameters from one set of solar cell devices. More statistical data from all the solar cells is shown in Figure S7 and Table S2 in the SI.

Table 1. PV representative parameter

Film	Jsc (mA/cm^2)	Voc (V)	FF	Efficiency (%)	R series (Ohm)	R Shunt (Ohm)
PS 2D	8.6	0.965	0.55	4.56	1.4 E-3	1.6 E+3
PS 2D-NT	14.4	0.995	0.63	9.03	9.5 E-2	1.8 E+3

PS 2D-G	10.7	0.945	0.61	6.17	1.3 E-3	1.4 E +3

Although this method resulted in lower power efficiencies than those achieved using hot deposition[31], addition of carbon nanotubes or graphene resulted in almost two-fold improvement in the performance when compared to pristine 2D perovskite. The increase in the grain size after adding SWCNTs contributed to improved photocurrent, in case of graphene, the grain size reduced but the crystallites orientation improved slightly, the future work to enhance power efficiency will require not only optimization of concentration of additives and its properties but also better understanding of their effect on grain size and crystallite orientation in 2D perovskite.

In summary, the carbon nanotubes provided an efficient transport media in the 2D perovskites, improving the charge-carrier lifetimes as shown by bulk optical property measurements and by two-dimensional mapping of the films. The effect on structure of 2D perovskite was studied using GISAXS and GIWAXS which showed the incorporation of the nanotubes led to larger vertical grain size. At cell level, addition of carbon nanotubes or graphene resulted in almost two-fold improvement in the performance when compared to pristine 2D perovskite. Thus, the use of SWCNT or graphene should be considered as a strategy to boost the power efficiency in less ordered 2D perovskite solar cells.

Experimental Methods

Two-dimensional perovskite films ($BA_2MA_3PbI_4I_{13}$) were prepared using a previously reported procedure[9]. SWCNTs (6,5 chirality, 0.78-nm diameter, 1-μm length, Sigma Aldrich) and single-layer graphene (thickness of 0.6–1.2 nm, flake diameter of 0.4–5 μm, ACS Material) were dispersed in dimethylacetamide (10 mM) and sonicated for 1 h. Blended solutions were prepared

by stirring overnight and deposited at room temperature by spin coating (2000 rpm, 15 s) and posterior annealing (120 °C, 10 min). Three-dimensional perovskite films ($CH_3NH_3PbI_3$) were prepared using lead acetate as a precursor.[22] Solar cells were fabricated by depositing PEDOT:PSS (Clevios Heraeus) on ITO substrates (1.5 × 1.5 cm) at 4000 rpm followed by 30-s annealing at 130 °C for 20 min. A PCBM film was used as the electron transport layer (20 mg/ml) in chlorobenzene (1000 rpm, 30 s); aluminum (100 nm) was evaporated as the electric contact.

Grazing-incidence wide-angle X-ray scattering measurements

GIWAXS experiments were performed at beamline 7.3.3 of the Advanced Light Source (ALS) at Lawrence Berkeley National Laboratory (LBNL). The X-ray energy was 10 keV, and the wavelength was 0.124 nm with a monochromator energy resolution E/dE of 100. The patterns were acquired using a two-dimensional (2D) Dectris Pilatus 2M CCD detector (172 μm × 172 μm pixel size). The scattering wave vector, $q = 4\pi \sin(\theta)/0.124$, ranged from 0.1 to 3.5 $Å^{-1}$ in WAXS configuration, where θ is the scattering angle. GIWAXS patterns were collected at grazing incidence angles, α_i of 0.20°, which is above the critical angle of the film and substrate. The exposure times for the collected images were 2, and all the films were imaged at ambient temperature in an enclosed helium box to ensure minimal background scattering and variation of the sample environment.

Optical measurements

Absorbance and transient photoluminescence measurements were performed using a Cary UV–vis–NIR and Horiba Jobin Yvon Fluorolog-3 spectrofluorometer with 500-nm source excitation.

The photoluminescence decay was measured using a Shimadzu UV-3600 spectrometer (UV/vis/NIR) with 500-nm laser excitation.

PL intensity and lifetime mapping were performed on a custom microscope built on a Nikon Eclipse Ti inverted microscope. The sample was illuminated with a Leukos super-continuum laser filtered to 520 nm which was focused to a diffraction limited spot with a Nikon 100x 0.95 NA objective. The sample was rastered with a MadCityLabs Piezo scan stage. Spectra were recorded with an Acton 2300i spectrometer and an Andor iXon EM-CCD. Lifetime signal were collected with an MPD PDM-series avalanche photodiode and recorded using PicoQuant PicoHarp 300 Timing electronics.

PV measurements

A solar simulator (model 71582, 150-W light source, Newport Oriel Instruments) was used for the PV measurements. Calibration was performed using a mono-Si cell at an irradiance of 1000 W/m^2 and device temperature of 24.7 °C.

ASSOCIATED CONTENT (Supporting Information)

Figure S1. Time-resolved photoluminescence decay of PS 2D ($BA_2MA_3Pb_4I_{13}$), and PS 2D alumina (Al_2O_3) nanoparticles under excitation at 500 nm.

Figure S2. GISAX results of PS 2D, PS 2D-NT, PS 2D G and PS 3D.

Figure S3. Scan –dependent current density (J)–potential (V) curves of perovskite solar cells PS 2D-NT, PS2D-G and PS 2D. Scanning rate of 10mV/s was used for forward (empty circles) and reverse (filled circles) scans.

Figure S4. Statistics of representative parameters showing effect of different carbon nanotubes concentration

Figure S5. Ultraviolet Photon Spectroscopy (UPS) measurements in PS 2D (black line), PS 2D-NT (red line), PS 2D-G (blue line).

Figure S6. Light intensity dependent variation in the A) open circuit voltage (Voc) and B) shunt resistance (Rsh) in the device.

Figure S7. Statistics data on Voc, fill factor and power efficiency from 40 solar cells of each type PS 2D, PS 2D-NT, PS2D-G.

Table S1. Trends in optical properties between samples

Table S2. Average PV parameters for 40 solar cells.

AUTHOR INFORMATION

msf@ier.unam.mx, Skaur1@lbl.gov

Notes

The authors declare no competing financial interest.

ACKNOWLEDGMENTS

This work was performed at Lawrence Berkeley National Laboratory. Work at the Molecular Foundry was supported by the Office of Science, Office of Basic Energy Sciences, of the U.S. Department of Energy under Contract No. DE-AC02-05CH1123. Work in the Energy Technologies Division was supported by CONACYT-SENER Mexico Energy Initiative: Mexican Postdoctoral Projects for Sustainable Energy Project No. 269386. Prof. Thomas P. Russell and Dr. Qin Hu were supported by the U.S. Office of Naval Research under Contract N00014-15-1-2244. The authors would also like to acknowledge Chenhui Zhu for his assistance with the use of equipment at beamline 7.3.3 at the Advanced Light Source (ALS).

REFERENCES

(1) Leijtens, T.; Bush K. A.; Prasanna R.; McGehee M. D. Opportunities and Challenges for Tandem Solar Cells Using Metal Halide Perovskite Semiconductors. *nature energy* **2018**, *3*, 828-838.

(2) Bryant D.; Aristidou N.; Pont S.; Sanchez-Molina I.; Chotchunangatchaval T.; Wheeler S.; Durrant J. R.; Haque S. A. Light and Oxygen Induced Degradation Limits the Operational Stability of Methylammonium Lead Triiodide Perovskite Solar Cells. *Energy Environ. Sci* **2016**, 9, 1655-1660.

(3) Zhang L.; Ju M. G.; Liang W. Z. The Effect of Moisture on the Structures and Properties of Lead Halide Perovskites: First-Principles Theoretical Investigation. *Phys. Chem. Chem. Phys*. **2016**, 18, 23174-23183.

(4) Divitini G.; Cacovich S.; Matteocci F.; Cina L.; Di Carlo A.; Ducati C. In situ Observation of Heat-Induced Degradation of Perovskite Solar Cells. *Nature energy* **2016**, 1, 15012-150217.

(5) Tsai H.; Nie W.; Blancon J. C.; Stoumpos C. C.; Asadpour R.; Harutyunyan B.; Neukirch A. J.; Verduzco R.; Crochet J. J.; Tretiak S.; Pedesseau L.; Even J.; Alam M. A.; Gupta G.; Lou J.; Ajayan P. M.; Bedzyk M. J.; Kanatzidis M. G.; Mothite A. D. High Efficiency Two-Dimensional Ruddlesden-Popper Perovskite Solar Cells. *Nature* **2016**, 536, 312-316.

(6) Lin Y.; Bai Y.; Fang Y.; Wang Q.; Deng Y.; Huang J. Suppressed Ion Migration in Low Dimensional Perovskites. *ACS Energy Lett*. **2017**, 2, 1571-1572.

(7) Etgar L. The Merit of Perovskites Dimensionality; Can This Replace the 3D Halide Perovskite. *Energy Environ. Sci*. **2018**, 11, 234-242.

(8) Tsai H.; Asadpour R.; Blancon J. C.; Stoumpos C. C.; Even J.; Ajayan P. M.; Kanatzidis M. G.: Alam M. A.; Mohite A. D. Design Principles for Electronic Charge Transport in Solution-Processed Vertically Stacked 2D Perovskite Quantum Wells. *Nat. Comm.* ***2018***, 9, 2130-2139.

(9) Chen A. Z.; Shiu M.; Ma J. H.; Alpert M. R.; Zhang D.; Foley B. J.; Smilgies D.; Lee S. H.; Choi J. J. Origin of Vertical Orientation in Two-Dimensional Metal Halide Perovskites and Its Effect on Photovoltaic Performance. *Nature Comm*. **2018**, 9, 1336-1343.

(10) Soe M.; Nie W.; Stoumpos C.C.; Tsai.; Blancon J.C.; Liu F.; Even J.; Marks T.J.; Mohite A.D.; Kanatzidis M.G. Understanding Film Formation Morphology and Orientation in High Member 2D Ruddlesden‐Popper Perovskites for High‐Efficiency Solar Cells. *Adv. Energy Mater* **2018**, 8, 1700979-1700989

(11) Zhang X.; Wu G.; Yang S.; Fu W.; Zhang Z.; Chen C.; Liu W.; Yan J. Yang W.; Chen H. Vertically Oriented 2D Layered Perovskite Solar Cells with Enhanced Efficiency and Good Stability. *Small* **2017**, 13,1700611- 1700619.

(12) Lian X.; Chen J.; Qin M.; Zhang Y.; Tian S.; Lu X.; Wu G.; Chen H. The second Spacer Cation Assisted Growth of a 2D Perovskite Film with Oriented Large Grain for Highly Efficient and Stable Solar Cells. *Angew. Chem. Int. Ed* **2019**, 58, 9409–9413.

(13) Blancon J. C.; Stier A.V.; Tsai H.; Nie W.; Stoumpos C. C.; Traore B.; Pedesseau L.; Kepenekian M.; Katsutani F.; Noe G. T.; Kono J.; Tretiak S.; Crooker S. A.; Katan C.; Kanatzidis M. G.; Crochet J. J.; Even J.; Mohite A. D. Scaling Law for Excitons in 2D Perovskite Quantum Wells. *Nature Comm* **2018**, 9, 2254-2264.

(14) Yang Y.; Yang M.; Li Z.; Crisp R.; Zhu K.; Beard M. C. Comparison of Recombination Dynamics in $CH_3NH_3PbBr_3$ and $CH_3NH_3PbI_3$ Perovskite Films: Influence of Exciton Binding Energy. *J. Phys. Chem. Lett*. **2015**, 6, 4688−4692.

(15) Blancon J. C.; Tsai H.; Nie W.; Stoumpos C. C.; Pedesseau L.; Katan C.; Kepenekian M.; Soe C. M.; Appavoo K.; Sfeir M.Y.; Tretiak S.; Ajayan P.M.; Kanatzidis M. G.; Even J.; Crochet J. J.; Mohite A.D. Extremely Efficient Internal Exciton Dissociation Through Edge States in Layered 2D Perovskites. *Science* **2017**, 355, 1288-1292.

(16) Habisreutinger S. N.; Nicholas, R. J.; Snaith H. J. Carbon Nanotubes in Perovskite Solar Cells. *Adv. Energy Mater.* **2017**, **7**, 1601839-1601846.

(17) Zhao X.; Tao L.; Li H.; Huang W.; Sun P.; Liu J.; Liu S.; Sun Q.; Cui Z.; Sun L.; Shen Y.; Yang Y.; Wang M. Efficient Planar Perovskite Solar Cells with Improved Fill Factor via Interface Engineering with Graphene. Nano Lett. **2018**, 18, 2442–2449.

(18) Schulz P.; Dowgiallo A. M.; Yang M.; Zhu K.; Blackburn J. L.; Berry J. J. Charge Transfer Dynamics between Carbon Nanotubes and Hybrid Organic Metal Halide Perovskite Films. *J. Phys. Chem. Lett.* **2016**,7, 418–425.

(19) Li F.; Wang F.; Kufer D.; Liang L.; Yu W.; Alarousu E.; Ma C.; Li Y.; Liu Z.;

Liu C.; Wei N.; Wang F.; Chen L.; Mohammed O. F.; Fratalocchi A.; Liu X.; Konstantanos G.; Wu T. Ultrahigh Carrier Mobility Achieved in Photoresponsive Hybrid Perovskite Films Via Coupling with Single-Walled Carbon Nanotubes. *Adv. Mater*. **2017**, 29, 1602432-1602440.

(20) Meng X.; Zhou J.; Hou J.; Tao X.; Cheung S. H.; So S. K.; Yang S. Versatility in Carbon Enables All Carbon Base Perovskite Solar Cells to Achieve High Efficiency and High Stability. *Adv. Mater.* **2018**, 30, 1706975-1706981.

(21) Li Y.; Leung W. W. Introduction of Graphene Nanofibers into the Perovskite Layer of Perovskite Solar Cells. *ChemSusChem* **2018**, 11, 2921-2929.

(22) Zhang W.; Saliba M.; Moore D.T.; Pathak S. K.; Hörantner M. T.; Stergiopoulos T.; Stranks S. D.; Eperon D. E.; Alexander-Webber J. A.; Abate A.; Sadhanala A.; Yao S.; Chen Y.; Friend R.H.; Estroff L. A.; Ulrich Wiesner U.; Snaith H. J. Ultrasmooth Organic–Inorganic Perovskite Thin-Film Formation and Crystallization for Efficient Planar Heterojunction Solar Cells. *Nat. Comm.* **2015**, 6, 6142-6152.

(23) Chen Y.; Sun Y.; Peng J.; Tang J.; Zheng K.; Liang Z. 2D Ruddlesden-Popper Perovskites for Optoelectronics. *Adv. Mater.* **2018**, 30, 1703487-1703502.

(24) Zheng K.; Chen Y.; Sun Y.; Chen J.; Chabera P.; Schaller R.; Al-Marri M. J.; Canton S. E.; Liang Z.; Pullerits T. Inter-phase Charge and Energy Transfer in Ruddlesden-Popper 2D Perovskites: Critical Role of the Spacing Cations. *J. Mater Chem. A* **2018**, 6,6444-6250.

(25) Liu B.; Soe C. M.; Stoumpos C. C.; Nie W.; Tsai H.; Lim K.; Mohite A. D.; Kanatzidis A.G.; Marks T. J.; Singer K. D. Optical Properties and Modeling of 2D Perovskite Solar Cells. *Sol RRL* **2017**, 1, 1700062-1700142.

(26) Milot R. L.; Sutton R. J.; Eperon G. E.; Haghighirad A. A.; Hardigree J. M.; Miranda L.; Snaith H. J.; Johnston M. B.; Herz L. M. Charge Carrier Dynamics in 2D Hybrid Metal-Halide Perovskite. *Nano Lett* **2016**, 16, 7001-7007.

(27) Xu J.; Buin A.; Ip A. H.; Li W.; Voznyy O.; Comin R.; Yuan M.; Jeon S.; Ning Z.; Jeffrey J. J.; Kanjanaboos P.; Sun J. P.; Lan X.; Quan L., Kim D. H.; Hill I. G.; Peter Maksymovych P.; Sargent E. H. Perovskite–Fullerene Hybrid Materials Suppress Hysteresis in Planar Diodes. Nat. comm. **2015**, 6, 7081-7089.

(28) Stranks S. D.; Burlakov V. M.; Leijtens T.; Ball J.M.; Gloriely A. Snaith H. J. Recombination Kinetics in Organic-Inorganic Perovskites: Excitons, Free Charge and Subgap States. *Phys. Rev. Applied. Chem* **2014**, 2, 034007.

(29) Barnard, E. S.; Ursprung B.; Colegrove E.; Moutinho H.; Borys N.J; Hardin B.E.; Peters C.H.; Metzger W.K.; Schuck, P.J. 3D Lifetime Tomography Reveals How CdCl2 Improves Recombination Throughout CdTe Solar Cells. *Adv. Mater*. **2017,** 29, 1603801-1603808

(30) Tsai H.; Nie W.; Blancon J. C.; Stoumpos C. C.; Asadpour R.; Harutyunyan B.; Neukirch A.J.; Verduzco R.; Crochet J. J.; Tretiak S.; Pedesseau L.; Even J.; Alam M.A.; Gupta G.;Lou J.; Ajayan P.M.; Bedzyck M.J. Kanatdzidis M.G.; Mohite A. D. High-efficiency two-dimensional Ruddlesden–Popper perovskite solar cells. *Nature*

2016, 536, 312-316.

(31) Kamat P. Best Practices in Perovskite Solar Cell Efficiency Measurements. Avoiding the Error of Making Bad Cells Look Good. *J. Phys. Chem. Lett.* **2015**, 6, 852−857.

(32) Hörantner M. T.; Nayak P.K.; Mukhopadhyay S.; Wojciechowski K.; Beck C. McMeekin D.; Kamino B.; Eperon G.E.; Snaith H. J. Shunt-Blocking Layers for Semitransparent Perovskite Solar Cells. *Adv. Mater. Interfaces* **2016**, 3, 1500837.